NaMoO2 : a layered oxide with molybdenum clusters

Laura Vitoux, Marie Guignard, Nicolas Penin, Dany Carlier-Larregaray, Jacques Darriet, Claude Delmas

$NaMoO_2$: a layered oxide with molybdenum clusters.

Laura Vitoux, Marie Guignard*, Nicolas Penin, Dany Carlier, Jacques Darriet, Claude Delmas

CNRS, Université de Bordeaux, Bordeaux INP, ICMCB UMR 5026, 33600 Pessac, France.

Supporting Information Placeholder

ABSTRACT: $NaMoO_2$ was synthesized as a layered oxide from the reaction between the layered oxide $Na_{2/3}MoO_2$ and metal sodium. Its structure was determined from high-resolution powder X-ray diffraction and it can be described as an α-$NaFeO_2$ distorted structure in which sodium ions and molybdenum atoms occupy octahedral interstitial sites. Chains of "diamond-like" clusters of molybdenum were evidenced in the $[MoO_2]$ layers resulting from the Peierls distortion expected in a two-dimensional triangular lattice formed by transition metal atoms with a d^3 electronic configuration. Molybdenum-molybdenum distances as short as 2.58 Å were found in these clusters. The magnetic moment recorded at low temperature and at room temperature showed that $NaMoO_2$ presents a very low magnetic susceptibility compatible with the localization of the 4d electrons in the Mo-Mo bonds. This localization was confirmed by DFT calculation that showed the NaMoO2 was diamagnetic at 0 K. A sodium battery was built using $NaMoO_2$ as the positive electrode material and we found that sodium ions can be reversibly deintercalated and intercalated in $NaMoO_2$ indicating that this compound is one of the many phases existing in the Na_xMoO_2 system.

1) Introduction

For a decade, sodium layered oxides Na_xMO_2 (M: 3d or 4d transition metal) are being revisited in search of new electron correlated materials. Their layered structure enables to tune the physical properties by intercalating or deintercalating sodium between the $[MO_2]$ layers made of edge-sharing MO_6 octahedra. The redox reaction, associated to the change in the sodium content, leads to modifications in the electronic properties. Moreover, the sodium/vacancy ordering, which can occur between the $[MO_2]$ layers for specific compositions due to electrostatic repulsions, can lead to a charge ordering within the $[MO_2]$ layers.[1] The electronic configuration of the M element (spin state, Jahn-Teller effect, tendency to form M-M bonds) plays also obviously an important role. Recently, our study of layered Na_xVO_2 phases shows that for the $Na_{1/2}VO_2$ composition there can be the formation of either vanadium dimers or vanadium trimers in three different polymorphs and that the existence of these clusters considerably effect the transport and the magnetic properties.[2-5] The existence of vanadium trimers was already found in $LiVO_2$ at room temperature associated to a low magnetic susceptibility.[6,7] More generally, the tendency for vanadium to form short V-V bonds is well known in vanadium oxides.[8,9] Molybdenum 3+ and 4+ are also well known to form direct bonds thanks to the overlapping of t_{2g} orbitals through edge-sharing MoO_6 octahedra.[10]

In the Na_xMoO_2 layered oxide system only three phases were obtained by solid-state synthesis: $Na_{2/3}MoO_2$,[11-14] $Na_{1/2}MoO_2$[15,16] and $NaMoO_2$.[17] Among these phases, the structure has only been reported for $Na_{1/2}MoO_2$ from single crystal X-ray diffraction and a specific arrangement of short Mo-Mo bonds (2.53 Å) in zig-zag chains separated from each other by long Mo-Mo distances (3.20 Å) has been found.[15] We have recently investigated the sodium electrochemical (de)intercalation in the $Na_{2/3}MoO_2$ phase and we have reported the existence of 16 single phases in the composition range: $0.3 \leq x < 1$.[18,19] The very small difference in composition and the reversibility of the (de)intercalation process suggest that these phases do not only differ from one to the other in the sodium patterning but also in the molybdenum clustering. Even though we could not solve any of their complex structure, one can expect to find molybdenum clusters within the $[MoO_2]$ layers, given the rich chemistry of molybdenum clusters observed in sulfurs, selenides, halogens and oxides.[20-23] The fully intercalated phase, $NaMoO_2$, has been the subject of a sole scientific paper 50 years ago reporting on its synthesis from the reaction of metal sodium on MoO_2 at 400 °C under vacuum.[17] Its structure, α-$NaFeO_2$ type structure, referred as an O3-type structure, according to Delmas's nomenclature,[24] is formed by three $[MoO_2]$ layers constituted of edge-sharing MoO_6 octahedra, between which sodium is intercalated in octahedral interstitial sites. However, the magnetic susceptibility measurements performed on this material revealed a Pauli paramagnetism, whose origin remains unclear. The existence of molybdenum clusters within the $[MoO_2]$ layers has been put forward by the authors. In this work, we decided to revisit the synthesis and the characterization of $NaMoO_2$. We developed a new synthesis method and we succeeded in obtaining for the first time highly crystalline $NaMoO_2$ which presents an original Mo-Mo bond network ("diamond-like" clusters) never reported in an oxide.

2) Experimental methods

$NaMoO_2$ synthesis was achieved by two synthesis routes. $NaMoO_2$ was synthesized by the reaction of metal sodium Na (30% excess compared to the stoichiometric ratio Na/MoO_2 = 1) on MoO_2 (Sigma Aldrich, 99%) in an open nickel crucible contained in a glass tube sealed under vacuum. It will be referred to $NaMoO_2$ (ex MoO_2) in the manuscript. $NaMoO_2$ (highly crystalline) was synthesized by the reaction of metallic sodium Na (30% excess compared to the stoichiometric ratio $Na/Na_{2/3}MoO_2$ = 1/3) on a $Na_{2/3}MoO_2$ powder (see below) in a nickel tube sealed under argon. It will be referred as $NaMoO_2$ (ex $Na_{2/3}MoO_2$) in the manuscript. For both syntheses, metallic sodium was cut in small cubes of approximately 10 mm^3 and it was gently mixed with the molybdenum oxides. Both products were obtained after the same heat treatment of 100 hours at 400°C. The excess of metal sodium was easily eliminated as

it condensed at one the extremities of the tubes, which was maintained at a slightly lower temperature during the cooling process. No trace of metal sodium was found in the obtained materials at the end of the heat treatments.

$Na_{2/3}MoO_2$ was synthesized by solid state reaction from the stoichiometric mixture of Na_2MoO_4, MoO_2 (Sigma Aldrich, 99%) and Mo (VWR, 99,9%), as previously reported for $Na_{2/3}MoO_2$.[12,14] Na_2MoO_4 was obtained by dehydration of the commercial product Na_2MoO_4, $2H_2O$ (VWR, 98%). The reactants were previously ground together by ball milling, 400 rpm/min for 3 hours, and heated in a gold tube sealed under argon at 700°C for 90 hours. The material was recovered in a glovebox under argon atmosphere to prevent oxidation and reaction with air moisture. It was obtained as a black powder.

High resolution X-ray powder diffraction was performed at the high resolution powder diffraction beamline (11-BM) at the Advanced Photon Source (APS) of the Argonne National Laboratory using a wavelength of 0.4142 Å, in the 0.5-50° 2θ range with a 0.001° step. NaMoO2 (ex $Na_{2/3}MoO2$) was loaded in a sealed 0.8 mm diameter Kapton capillary sealed with epoxy. Structure refinements using the Rietveld method were carried out using Jana2006 program.[25]

Pair distribution functions (PDFs) were generated for $NaMoO_2$ (ex MoO_2) from X-ray powder diffraction data recorded at 11-ID-B beamline at the APS using a wavelength of 0.2114 Å. The diffraction data recorded on an empty Kapton capillary in the same conditions have been used to correct the diffracted intensity from the background. The measured diffracted intensity has been corrected from the incoherent scattering, the background, the polarization and the absorption using the ad-hoc method provided by PDFgetX3 software.[26] The corrected intensity I(Q) and the structure function S(Q) have been calculated using this program, with $Q = 4\pi\sin\theta/\lambda$. Reduced PDFs G(r) have been obtained by Fourier transforming S(Q) functions over the 0.5-24 $Å^{-1}$ Q-range. Calculated PDFs have been obtained using the PDFgui software.[27]

Electrochemical studies were carried out on Na | $NaPF_6$ + 2% fluoroethylene carbonate (FEC) in propylene carbonate (PC) (1M) | Na_xMoO_2 batteries assembled in airtight 2032 type coin cells. At the positive electrode, the active material was mixed with carbon black to improve its electronic conduction and with PTFE (polytetrafluoroethylene) used as binder in a 88:10:2 weight ratio. Sodium batteries were galvanostatically charged and discharged at C/100 rate (1 Na^+ per formula unit (de)intercalated in 100 hours) between 1.7 V and 3.5 V.

For transport measurements, sintered pellets of $NaMoO_2$ (ex $Na_{2/3}MoO_2$) were used in an air-tight apparatus and the electrical resistance was measured using the four-probe technique in the 77-300 K temperature range. The resistance of the pellet was measured while it was continuously heated up. $NaMoO_2$ pellets were obtained by reacting sodium metallic on 8 mm $Na_{2/3}MoO_2$ pellets in a nickel crucible contained in a glass tube sealed under vacuum.

Magnetic Measurement were made on a SQUID magnetometer on approximately 40 mg of $NaMoO_2$ (ex $Na_{2/3}MoO_2$) powder. The magnetic susceptibility was measured in an applied field of 1 kOe between 5 and 100K (ZFC/FC). The correction of the diamagnetic contribution was evaluated using Pascal's constant.

Total energies and electronic structure have been calculated within GGA (PBE),[28] using the Projector Augmented Wave (PAW) method[29] as implemented in the Vienna Ab Initio Simulation Package (VASP).[30] A plane wave cutoff energy of 500 meV and a 6x6x6 k-point grid was used for the $NaMoO_2$ cells to let the total energy converge by less than 5 meV/unit cell. The atomic positions and the lattice parameters of the experimental cell were fully relaxed using a spin polarized approach. For the plot of the partial DOS around Mo, a sphere radius of 0.6 Å was used for the integration. The method developed by R. Bader to divide molecules into atoms was used in order to determine partial charges on Mo ions.[31] The implementation of this method to the VASP output is described in reference.[32-34] The Electron Localization Function (ELF)[35] is directly available from the *VASP* code[30] The VESTA code was used to plot the 3D spin or ELF maps.[36]

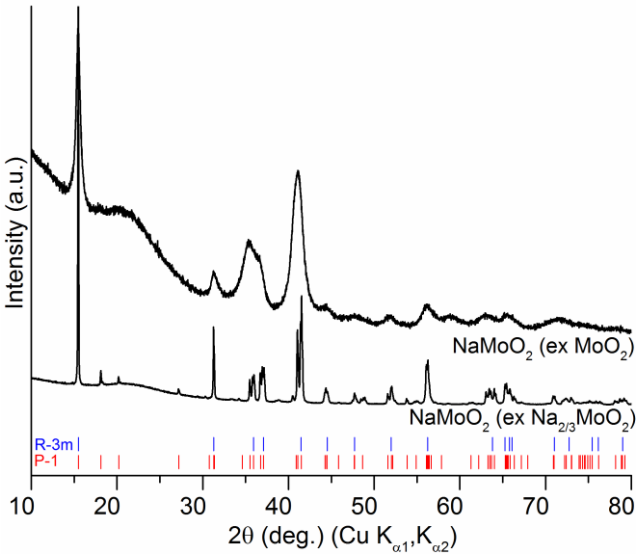

Figure 1. Powder X-ray diffraction patterns of $NaMoO_2$ (ex MoO_2) (top) and $NaMoO_2$ (ex $Na_{2/3}MoO_2$) (bottom). Bragg peak positions are given for two unit cells. In blue: a = 2.95 Å, c = 16.95 Å (Space group: R-3m). In red: a = 5.1067 Å, b = 2.9056 Å, c = 5.9655 Å, α = 90.157°, β = 106.745°, γ = 89.651° (Space group: P-1).

3) Results and discussion

In a first step $NaMoO_2$ material was synthesized by reacting metallic sodium with MoO_2 powder under vacuum, as previously reported.[17] Its powder X-ray diffraction pattern exhibits however very large diffraction peaks, making difficult a precise structural characterization (Figure 1). Nevertheless it can be indexed in a first approach using the unit cell of an O3-type structure with the space group R-3m and cell parameters a ≈ 2.95 Å and c ≈ 16.95 Å. Pair function distribution (PDF) analysis were then undertaken to obtain information on the local structure and especially on the molybdenum environment. The experimental G(r) is shown in Figure 2.a. The calculated G(r) function, based on the ideal hexagonal O3-type structure, is superimposed on the experimental one (Figure 2.b). Significant differences between the two functions question the validity of the published model. Moreover, the rapid loss of intensity and peaks resolution observed on the experimental G(r) function suggests the presence of high degree of disorder. Finally, the experimental intensity becomes non-existent for

correlation distances r > 40 Å suggesting nano-sized coherent domains. Structural disorder and nano-sized domains both lead to the broadening of the peaks on the X-ray diffraction pattern.

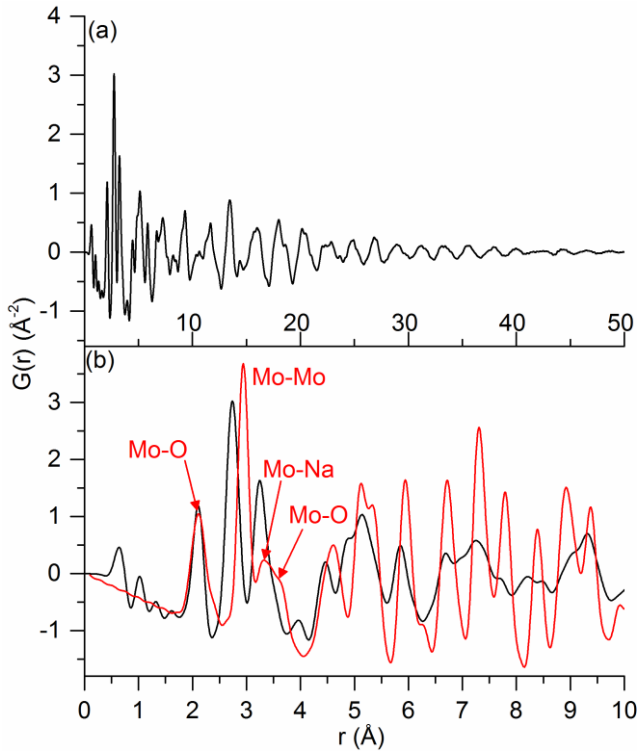

Figure 2. (a) and (b) Experimental reduced pair distribution function (PDF), G(r), of $NaMoO_2$ (ex MoO2) (in black). (b) Calculated G(r) of NaMoO2 considering an O3-type structure with the cell parameters a = 2.95 Å, c = 16.95 Å (Space group: R-3m) (in red).

Crystal growth by thermal annealing was attempted to enhance the quality of the X-ray diffraction pattern in order to propose a new structural model using the Rietveld method. Unfortunately, thermal treatment above 475°C results in the decomposition of $NaMoO_2$ into Mo and Na_2MoO_4 due to the tendency of Mo^{3+} to dismute into Mo^0 and Mo^{6+}. Another synthesis method was therefore undertaken to obtain a highly crystalline $NaMoO_2$ powder.

As part of the investigation of the Na_xMoO_2 system, a well-crystallized pristine material $Na_{2/3}MoO_2$ has been synthesized by solid state synthesis. The sodium electrochemical intercalation or deintercalation in a sodium battery made with this material as the positive electrode has been used as a powerful technique to explore the phase diagram in the $NaMoO_2$-MoO_2 system.[14,18,19] More specifically, our *in situ* X-ray diffraction experiment performed during sodium electrochemical intercalation showed that a composition close to Na_1MoO_2 existed at very low voltage (< 1V vs Na^+/Na).[18] Nevertheless, the organic liquid electrolyte ($NaPF_6$ in propylene carbonate) was not stable at this low voltage and it decomposed before all the Na_xMoO_2 (x ≈ 0.9) phase could be transformed into $NaMoO_2$, making the electrochemical method not adequate for $NaMoO_2$ preparation. Chemical sodium intercalation in soft conditions from $Na_{2/3}MoO_2$ was therefore considered to obtain highly crystalline $NaMoO_2$.

Chemical intercalation of sodium ions between the $[MoO_2]$ layers of the $Na_{2/3}MoO_2$ structure has been achieved by reacting sodium metal on the pristine material at 400°C. The X-ray diffraction pattern of the obtained black powder presents sharp diffraction peaks, indicating a high degree of crystallinity of the material (Figure 1). The hexagonal cell (Space group: R-3m) reported in 1969 for the structure of $NaMoO_2$ (ex MoO_2) cannot allow a correct indexation of the X-ray pattern of $NaMoO_2$ (ex $Na_{2/3}MoO_2$). For each Bragg peak generated in this space group, actual diffraction peaks seem to be split indicating a lowering of the symmetry. Monoclinic distortions are common in sodium layered oxides and result generally from Jahn-Teller effect or slab gliding or sodium/vacancy orderings or metal-metal bonding during sodium electrochemical (de)intercalation. An O3-type structure is then described in a C2/m space group and denominated O'3.[37] However, in this case, a monoclinic cell cannot allow a correct indexation of the X-ray diffraction pattern of $NaMoO_2$ (ex $Na_{2/3}MoO_2$) (See Supporting Information). A triclinic distortion of the corresponding monoclinic cell was then considered with alpha and gamma varying slightly from 90° (a = 5.1067(2) Å, b = 2.9056(1) Å, c = 5.9655(3) Å, α = 90.157(4) °, β = 106.745(3) °, γ = 89.651(3) °). The Bragg peak positions of the triclinic cell (Space group: P-1) are indicated by red ticks and they enable to index all the main peaks on the X-ray diffraction pattern of $NaMoO_2$ (Figure 1)

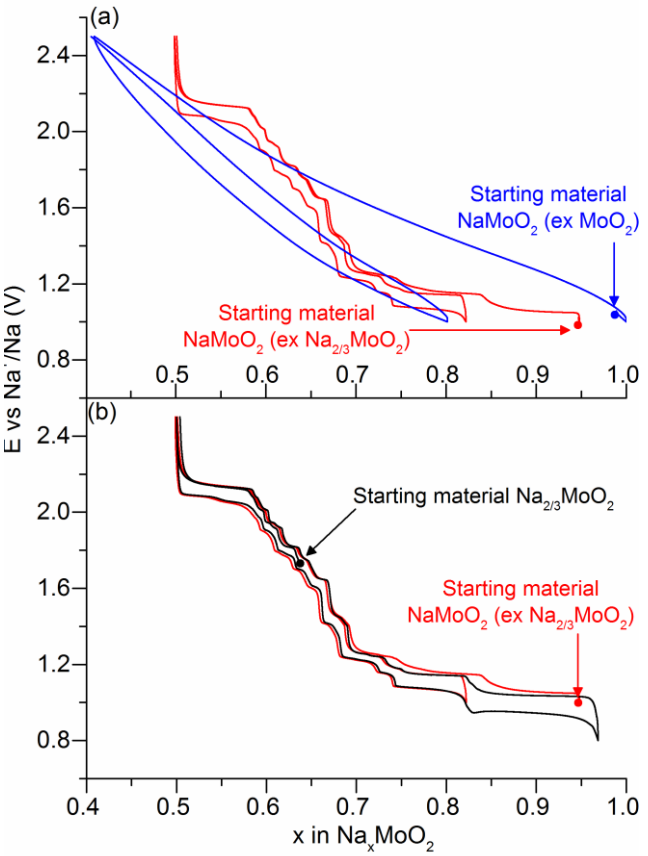

Figure 3. First galvanostatic cycle of electrochemical sodium cells made with Na_xMoO_2 phases as the positive electrode material. (a) With $NaMoO_2$ (ex MoO_2) (in blue) and with $NaMoO_2$ (ex $Na_{2/3}MoO_2$) (in red). (b) With $Na_{2/3}MoO_2$ (in black) and with $NaMoO_2$ (ex $Na_{2/3}MoO_2$) (in red).

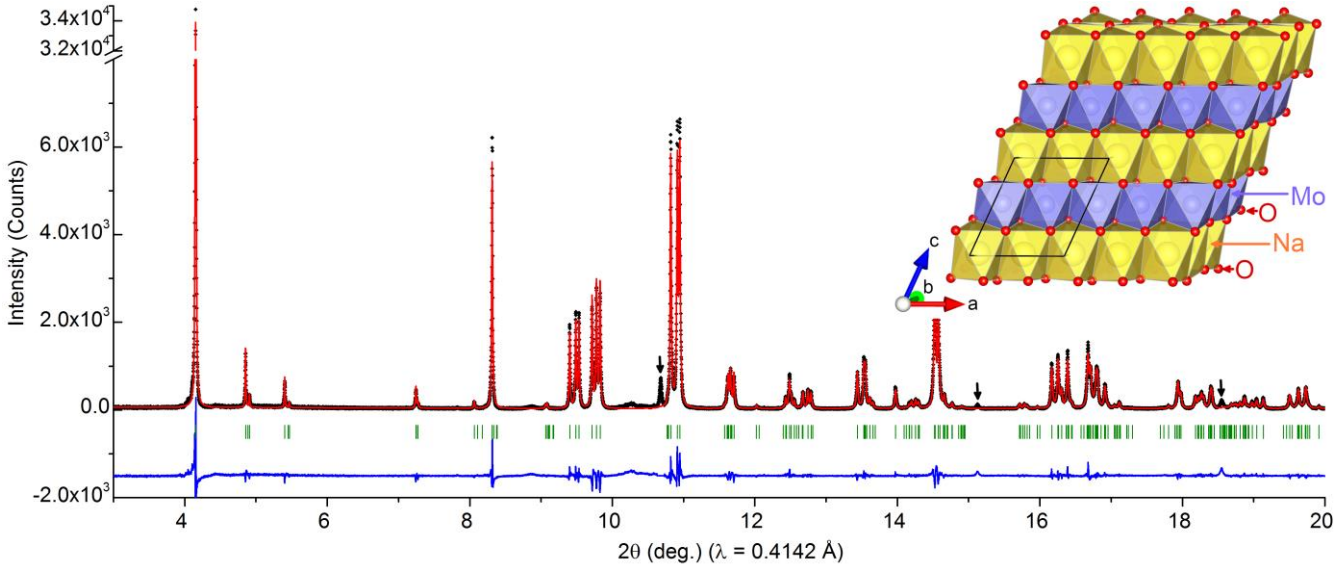

Figure 4. Experimental high resolution X-ray powder diffraction pattern of $NaMoO_2$ (ex $Na_{2/3}MoO_2$) (black diamonds), calculated pattern obtained from the Rietveld refinement (red line) considering the O"3 triclinic cell with the cell parameters: a = 5.8113 Å, b = 5.8603 Å, c = 6.6291 Å, α = 63.907 °, β = 64.154 °, γ = 60.620 °. The difference between the calculated pattern and the experimental one is shown by the blue line. Green vertical bars show the position of the Bragg reflections for the O3" triclinic cell. The inset shows a three-dimensional representation of the structure of $NaMoO_2$ (ex $Na_{2/3}MoO_2$) obtained from the Rietveld refinement. Black arrows indicate diffraction peaks for molybdenum metal impurity.

Both $NaMoO_2$ phases, obtained from either MoO_2 or $Na_{2/3}MoO_2$, were used as positive electrode materials in sodium batteries. Galvanostatic electrochemical curves present in Figure 3 the evolution of the cell voltage as a function of the sodium amount x in the layered phase Na_xMoO_2. Structural differences between the two $NaMoO_2$ materials, highlighted by X-ray diffraction, lead to significant differences on the electrochemical responses of the two phases (Figure 3.a). The high structural disorder in $NaMoO_2$ (ex MoO_2), suggested by both the broadening of the diffraction peaks and the loss of correlation on the G(r) function, prevents any orderings (sodium/vacancy ordering or molybdenum clustering). Therefore, the smooth aspect of the electrochemical curve, characteristic of a solid solution behavior, indicates that no phase transition occurs upon sodium electrochemical deintercalation.

On the other hand, the electrochemical curve recorded for $NaMoO_2$ (ex $Na_{2/3}MoO_2$) is more complex with several voltage drops and plateaus, very similar to those observed on the electrochemical galvanostatic curve of the sodium battery made with $Na_{2/3}MoO_2$ as the positive electrode (Figure 3.b). This indicates that the sodium chemical intercalation in $Na_{2/3}MoO_2$ is highly effective to maintain the layered host structure to form $NaMoO_2$. It should be noticed however that the initial voltage of the battery made with $NaMoO_2$ (ex $Na_{2/3}MoO_2$) does not correspond to the fully intercalated material x = 1. It lies on the voltage plateau between $Na_{0.82}MoO_2$ and $NaMoO_2$. This initial loss of sodium probably results from the reaction of the very reductive $NaMoO_2$ with the electrolyte when the battery was first assembled in the glovebox.

The structure of $NaMoO_2$ (ex $Na_{2/3}MoO_2$) was determined from the high-resolution X-ray powder diffraction data using the Rietveld method (Figure 4). Due to the high signal to noise ratio achieved at the synchrotron, several diffraction peaks are visible at small angles. They can be indexed using a supercell resulting from the doubling of the monoclinic cell parameters in the three directions a, b and c. However, this lead to numerous Bragg reflections, for which there is no diffracted intensity. A smaller triclinic cell (a = 5.8113(2) Å, b = 5.8603(3) Å, c = 6.6291(4) Å, α = 63.907(3) °, β = 64.154(3) °, γ = 60.620(3) °) was then found to index each superstructure peaks without generating any superfluous reflections. The relationship between the initial monoclinic cell and the final triclinic supercell is described in Supplementary Information (Figure S1). Structural parameters determined from the Rietveld refinement are reported in supporting Information in Table S1.

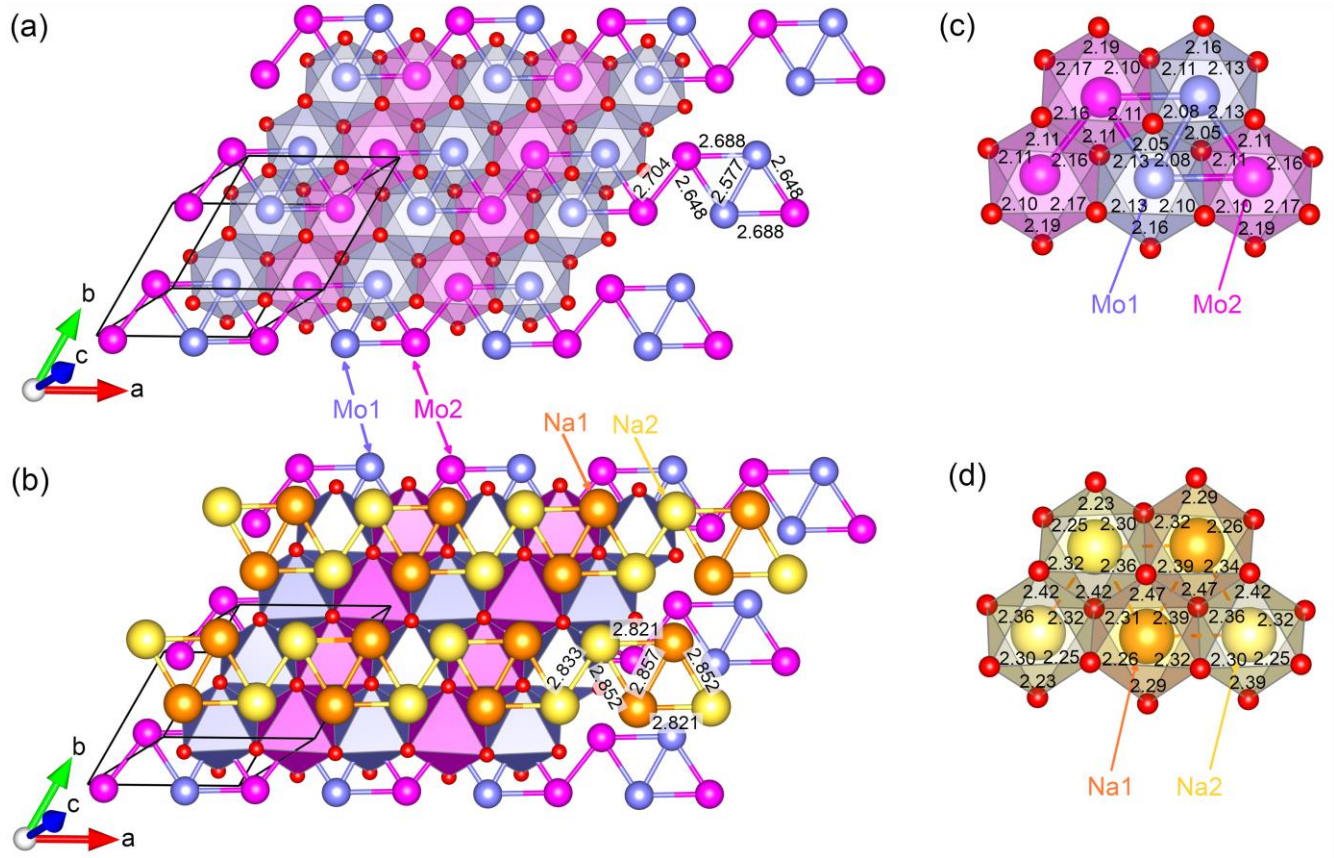

Figure 5. Projection of the structure of $NaMoO_2$ parallel to the $[MoO_2]$ layers. (a) Single $[MoO_2]$ layer made of MoO_6 octahedra highlighting the existence of "diamond-like" clusters. Mo-Mo bonds are reprented by pink-purple bicolor solid sticks and shortest Mo-Mo distances are given in Å. (b) Same as (a) with a single layer of Na^+ ions on top of the $[MoO_2]$ layer. Shortest Na^+-Na^+ distances are reprented by yellow-orange bicolor solid sticks. The values of these distances are given in Å. (c) Mo-Mo distances given in Å. (d) Na-O distances given in Å. Oxygen atoms are represented by red circles and the limits of the O"3 triclinic unit cell are shown with solid black lines.

The structure can be described as a distorted O3-type structure in which sodium fully occupies octahedral interstitial sites sharing edges with MoO_6 octahedra in the $[MoO_2]$ slabs (Inset Figure 4). This triclinic structure will be referred as O"3-type structure in the following text. The interesting feature of this structure is the displacement of the molybdenum atoms from the center of MoO_6 octahedra to form shorts Mo-Mo bonds (Figure 5.c). MoO_6 octahedra are also distorted leading to a slight undulation of the $[MoO_2]$ layers. As it could be expected $4d^3$ cation, each Mo^{3+} ion forms three short Mo-Mo bonds with their neighboring Mo^{3+} ions resulting in infinite chains of diamond-like clusters along the a-axis (Figure 5.a). Such metal clustering would be due to a Peierls distortion associated with the partial occupation of the t_{2g} block for d^3 metal ions.[38] The shortest Mo-Mo bond, $d_{Mo1\text{-}Mo1}$ = 2.577 Å, is in the center of the diamond shaped by Mo1-Mo2 bonds, $d_{Mo1\text{-}Mo2}$ = 2.648 Å and 2.688 Å. "Diamond-like" clusters are linked together by the slightly longer Mo2-Mo2 bond ($d_{Mo2\text{-}Mo2}$ = 2.704 Å). Chains are separated by long Mo-Mo distances of approximately 3.2 Å. Between the $[MoO_2]$ layers, sodium ions are also slightly shifted off the center of the NaO_6 octahedra to minimize Na^+/Mo^{3+} repulsions (Figure 5.d). It results in short (~ 2.82 Å and 2.85 Å) and long (~ 3.0 Å) Na-Na distances, which form the same pattern as Mo-Mo bonds within the $[MoO_2]$ slabs, but shifted to minimize electrostatic repulsions (Figure 5.c). The driving force of this unusual sodium arrangement is the formation of the Mo-Mo clusters.

Similar metallic clusters were observed in sulfides where the transition metal has a d^3 electronic configuration, like molybdenum in $NaMoO_2$. It was first reported for ReX_2 (X = S, Se)[39-43] and TcS_2[39,41] and then for MMo_2S_4 (M=Co,Fe),[44] Mo_2S_3,[45] and $LiMoS_2$.[46,47] Theoretical calculations confirmed that the metal arrangement to form "diamond-like" clusters was favorable in ReX_2 (X = S, Se),[48-50] $LiMoS_2$[51] and $NaMoS_2$.[52] In all cases, the interlayer space is either empty or fully occupied confirming that the origin of the "diamond-like" clusters is the $4d^3$ or $5d^3$ electronic configuration of the transition metal. This molybdenum arrangement has never been observed in $LiMoO_2$, which also contains Mo^{3+} ions.[53-56] More precisely, the existence of molybdenum zig-zag chains has been evidenced by EXAFS[55] and neutron diffraction and total neutron scattering.[56] As ionic radii of Mo^{3+} (r_i = 0.69 Å) and Li^+ (r_i = 076 Å) are close,[57] there is a mixed occupancy of Mo and Li within the $[MoO_2]$ layers. This prevents from a long range ordering of the molybdenum atoms within the $[(Mo, Li)O_2]$ layers, and it induces an uncertainty on the oxidation state of the molybdenum.[58] In $NaMoO_2$, because Na^+ ions are significantly larger than Mo^{3+} (r_i(Na+) = 1.02 Å), we think that no Na/Mo mixing occurs and that the $[MoO_2]$ layers are free of sodium. Na/Mo mixing would smooth the galvanostatic electrochemical curve

as it is the case for electrochemical curves recorded for lithium batteries using $LiMoO_2$ as the positive electrode material.[58]

To the best of our knowledge, this is the first time that such "diamond-like" Mo clustering is observed in an oxide. To ensure that the structural description resulting from the Rietveld refinement based on the X-ray powder diffraction data was correct, structural optimization by DFT calculations were performed. Subsequently, the study of the electronic structure of $NaMoO_2$ (ex $Na_{2/3}MoO_2$) was performed.

The cell parameters and atomic positions were fully relaxed using GGA starting from the experimental parameters given in Table S1. As seen in Table S2 (See Supporting Information), the optimized structure is in good agreement with the experimental data. In particular, the "diamond-like" Mo clustering is maintained and the oxygen atomic positions found from X-ray powder diffraction are confirmed. The optimized Mo-Mo distances are given Table S3 (See Supporting Information) and they are in good agreement with the experimental values. The energy of a hypothetical O3-$NaMoO_2$ cell without Mo clusters (Space group: R-3m) was also computed in order to get a sense of the stability increase induced by the cluster formation. It appears that the "diamond-like" Mo clusters strongly stabilized the phase by 600 meV per formula unit. For $LiMoS_2$, the stabilization of the "diamond–like" chains was also reported due to a charge density wave (CDW) using FP-LAPW calculations.[51] The DOS modelling of an undistorted O3-$NaMoO_2$ phase was also recently reported, without considering possible Mo clusters formation.[59]

Even if we initiated spin polarized DFT calculations using initial magnetic moment on Mo sites, the calculations converged to a diamagnetic solution, with equivalent "up" and "down" states due to the formation of Mo-Mo bonds and electron pairing. All the calculations made using the GGA + U method, even with a U value as low as 2 eV applied to the Mo d orbitals, led to a disappearance of the molybdenum clusters. In order to investigate the electronic structure of $NaMoO_2$, the total Density of States (DOS) and partial DOS on Mo ions are presented in Figure 6. Note that the partial DOS of the two molybdenum ions in the structure are quite similar, as well as the Bader charges (around +1.44). A 1.1 eV electronic gap is calculated using GGA for this material.

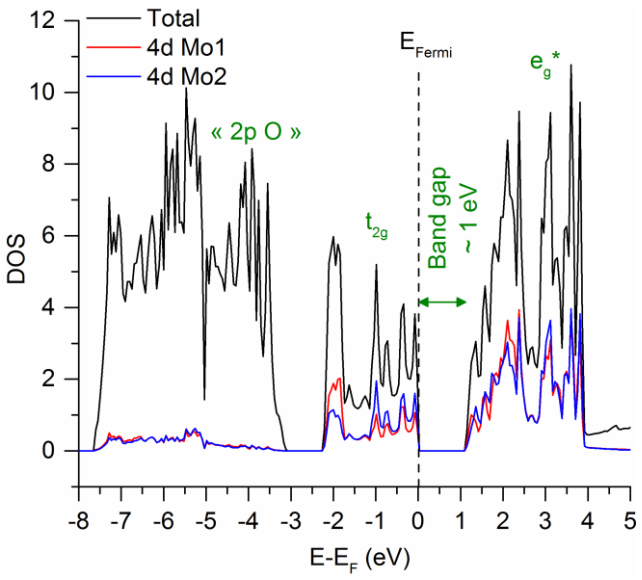

Figure 6. Total and partial Density of State (DOS) calculated for $NaMoO_2$ (ex $Na_{2/3}MoO_2$).

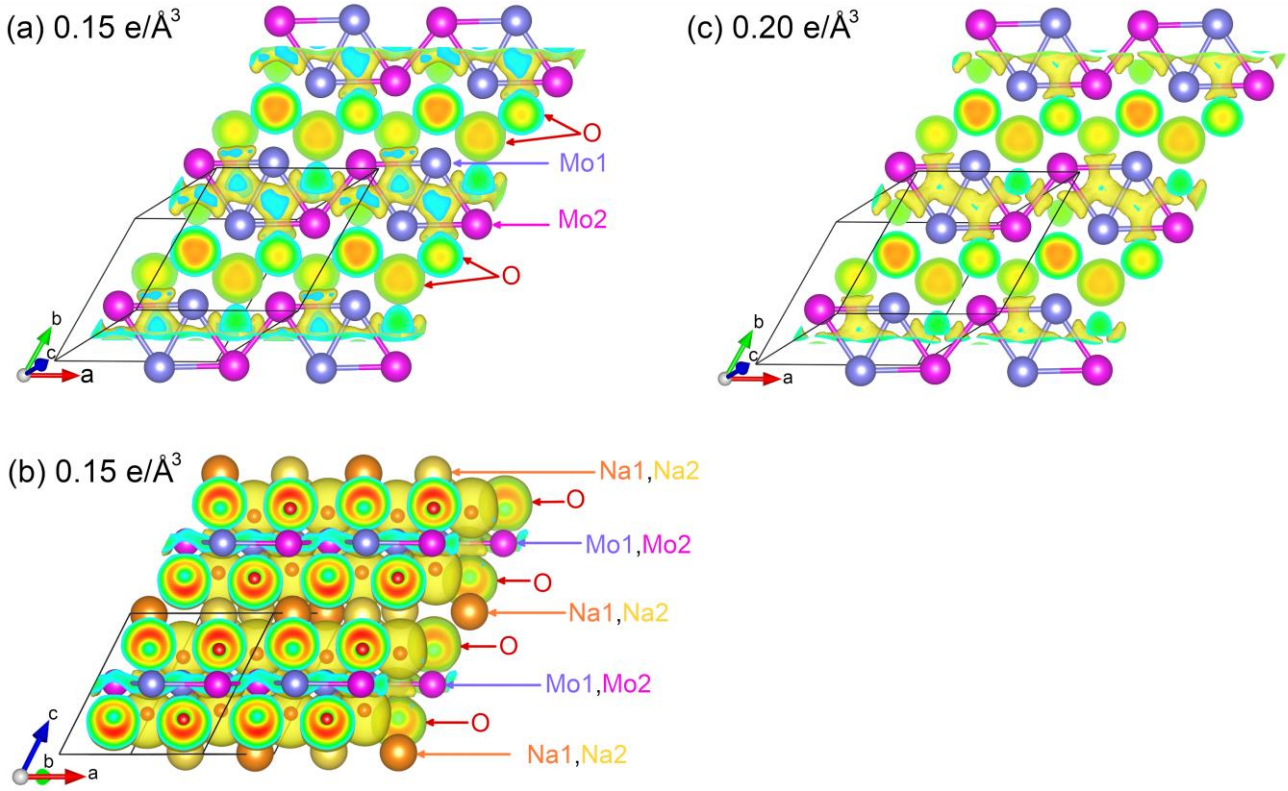

Figure 7. Electron Localization Function (ELF) three-dimensional maps. (a) and (b) With an isotropic surface value of 0.15 e/Å^3. (c) With an isotropic surface value of 0.20 e/Å^3.

Calculated Electron Localization Function (ELF) 3D maps are shown in Figure 7 were plotted using two different isotropic surface values and different orientation, in order to visualize the Mo-Mo bonds.Strong electronic density clearly appears in between the molybdenum ions forming the "diamond-like" cluster chains along the a-direction, and none between those cluster chains. Note that the electronic density is not equivalent between all molybdenum ions: it is stronger between Mo forming the "diamond-like" figure and weaker between Mo of adjacent "diamond" in agreement with the experimental and calculated bond lengths. The presence of electronic density nearby the center of the Mo triangles of the diamond is due to the recombination of the t_{2g} orbitals stabilizing the system.

The formation of Mo-Mo bonds within the [MoO_2] layers should influence the physical properties of the material. The measurement of the magnetic susceptibility showed a low paramagnetism (Figure S2). This is in agreement with the proposed structure of chains of "diamond-like" Mo clusters and this is coherent with the diamagnetic properties determined at 0 K from DFT calculations. According to resistivity measurements, $NaMoO_2$ is a semi-conducting material (E_a = 0.122 eV) with a low conductivity at ambient temperature (σ = 2.4.10^{-4} S.cm^{-1}) (Figure S3). Similar semi-conducting properties were reported for $MMoS_4$ (M = Fe, Co) and a mechanism of charge hopping along the short Mo-Mo bonds was suggested.[44] Both magnetic and electronic characterizations are in good agreement with the proposed structure. In addition, no electronic or magnetic transition was observed below room temperature, indicating a good stability of this molybdenum arrangement at low temperature.

4) Conclusion

Highly crystalline $NaMoO_2$ was synthesized for the first time and its structure was solved using the Rietveld method based on high resolution X-ray powder diffraction. Chains of "diamond-like" clusters of molybdenum were evidenced in the [MoO_2] layers resulting from the Peierls distortion expected in a two-dimensional triangular lattice formed by transition metal atoms with a d^3 electronic configuration. It is to our knowledge the first time that this metal clustering has been found in an oxide. Its stability was confirmed by DFT calculations.

Sodium electrochemical deintercalation from $NaMoO_2$ in a sodium battery lead to the formation of several Na_xMoO_2 layered phases with specific composition, highlighted by voltage drop on the multiple-step electrochemical curve. This curve is very similar to the one recorded for a battery made of $Na_{2/3}MoO_2$ as the positive electrode. In conclusion, the structural characterization of $NaMoO_2$ gives valuable information on the Na_xMoO_2 phase diagram and a new example of transition metal ordering in the [MoO_2] layers that can occur upon cycling, since no structure apart from that of $Na_{1/2}MoO_2$ has been reported yet.

ASSOCIATED CONTENT

Supporting Information

The relationship between the initial monoclinic cell and the final triclinic supercell is described in Supporting Information. The cell parameters and atomic positions relaxed using GGA starting from the experimental parameters are given in Supporting Information. Evolution of the magnetic susceptibility and of the electronic resistivity as a function of the temperature are given Supporting Information. This material is available free of charge via the Internet at http://pubs.acs.org.

AUTHOR INFORMATION

Corresponding Author

Marie GUIGNARD, marie.guignard@icmcb.cnrs.fr.

Author Contributions

The manuscript was written through contributions of all authors. All authors have given approval to the final version of the manuscript.

Funding Sources

This work was supported by the Agence Nationale de la Recherche through the grant ANR-14-CE05-0011. This research used resources of the Advanced Photon Source, a U.S. Department of Energy (DOE) Office of Science User Facility operated for the DOE Office of Science by Argonne National Laboratory under Contract No. DE-AC02-06CH11357.

ACKNOWLEDGMENT

MG would like to thank Olag Borkiewicz from the Advanced Photon Source for collecting the pair distribution function data.

REFERENCES

(1) Roger, M.; Morris, D. J. P.; Tennant, D. A.; Gutmann, M. J.; Goff, J. P.; Hoffmann, J.-U.; Feyerherm, R.; Dudzik, E.; Prabhakaran, D.; Boothroyd, A. T.; Shannon, N.; Lake, B.; Deen, P. P. Patterning of Sodium Ions and the Control of Electrons in Sodium Cobaltate. *Nature* **2007**, *445 (7128)*, 631–634.

(2) Didier, C., Guignard, M., Darriet, J. & Delmas, C. O′3–Na_xVO_2 System: A Superstructure for $Na_{1/2}VO_2$. *Inorg. Chem.* **2012**, *51*, 11007–11016.

(3) Guignard, M.; Dider, C.; Darriet, J.; Bordet, P.; Elkaïm, E.; Delmas, C. P2-Na_xVO_2 System as Electrodes for Batteries and Electron-Correlated Materials. *Nat. Mater.* **2013**, *12*, 74–80.

(4) Guignard, M.; Carlier, D.; Didier, C.; Suchomel, M. R.; Elkaïm, E.; Bordet, P.; Decourt, R.; Darriet, J.; Delmas, C. Vanadium Clustering/Declustering in P2–$Na_{1/2}VO_2$ Layered Oxide. *Chem. Mater.* **2014**, *26* (4), 1538–1548.

(5) Guignard, M.; Delmas, C. Using a Battery to Synthesize New Vanadium Oxides. ChemistrySelect 2017, 2, 5800–5804.

(6) Imai, K.; Sawa, H.; Koike, M., Hasegawa, M.; Takei, H. Superstructure Analyses on Single Crystals of $Li_{0.8}VO_2$. *J. Solid State Chem.* **1995**, *114*, 184–189.

(7) Pourpoint, F.; Hua, X. ; Middlemiss, D. S.; Adamson, P.; Wang, D.; Bruce, P. G.; Grey C. P. New Insights into the Crystal and Electronic Structures of $Li_{1+x}V_{1-x}O_2$ from Solid State NMR, Pair Distribution Function Analyses, and First Principles Calculations. *Chem. Mater.* **2012**, *24*, 2880–2893.

(8) Longo, J. M.; Kierkegaard, P. A. Refinement of the Structure of VO_2. *Acta Chem. Scand.* **1970**, *24*, 420–426.

(9) Dernier, P. D. The Crystal Structure of V_2O_3 and $(V_{0.962}Cr_{0.038})_2O_3$ near the Metal-Insulator Transition. J. Phys. Chem. Solids 1970, 31, 2569–2575.

(10) Burdett, J. K.; Hughbanks, T. Aspects of Metal-Metal Bonding in Early-Transition-Metal Dioxides. *Inorg. Chem.* **1985**, *24 (12)*, 1741–1750.

(11) Hubert, P.-H. Sur l'Obtention du Molybdite de sodium. *C. R. Acad. Sc. Paris, Série C* **1966**, *262*, 1189–1191.

(12) Réau, J.-M.; Fouassier, C.; Hagenmuller, P. Les Systèmes MoO_2-A_2O et WO_2 -A_2O (A = Li, Na, K). *Bull. Soc. Chim. Fr.*, **1970**, *11*, 3827–3829.

(13) Hirano, S.; Kozima, M.; Naka, S. Hydrothermal Synthesis and Properties of Na_xMoO_2 Single Crystal. *Toyota Kenkyu Hokoku* **1984**, *37*, 32–38.

(14) Tarascon, J. M.; Hull, G. W. Sodium Intercalation into the Layered Oxides $Na_xMo_2O_4$. *Solid State Ion.* **1986**, *22*, 85–96.

(15) McCarley, R. E.; Lii, K.-H.; Edwards, P. A.; Brough, L. F. New Extended Clusters in Ternary Molybdenum Oxides. *J. Solid State Chem.* **1985**, *57*, 17–24.

(16) Aleandri, L. E. Synthesis and characterization of reduced ternary alkali metal molybdenum oxides. Iowa State University (1987).

(17) Ringenbach, C.; Kessler, H.; Hatterer. A. Un Nouveau Composé Oxygéné du Molybdène $NaMoO_2$. Propriétés Cristallographiques et Magnétiques. *C. R. Acad. Sc. Paris, Série C* **1969**, *269*, 1394–1397.

(18) Vitoux, L; Guignard, M.; Suchomel, M. R.; Pramudita, J. C.; Sharma, N.; Delmas, C. The Na_xMoO_2 Phase Diagram ($^1/_2 \leq x < 1$): An Electrochemical Devil's Staircase. *Chem. Mater.* **2017**, *29 (17)*, 7243–7254.

(19) Vitoux, L. ; Guignard, M.; Darriet, J.; Delmas, C. Exploration of the Na_xMoO_2 phase diagram for low sodium contents (x ≤ 0.5). *J. Mater. Chem. A* **2018**, *6*, 14651–14662.

(20) Tkachenko, E. A. & Fedorov, P. P. Lower Rare-Earth Molybdates. *Inorg. Mater.* **2003**, *39*, S25–S52.

(21) Simon, A. Metal clusters inside out. Philos. Trans. R. Soc. A-Math. Phys. Eng. Sci. **2010**, 368, 1285–1299.

(22) Sokolov, M. N., Naumov, N. G., Samoylov, P. P. & Fedin, V. P. in *Comprehensive Inorganic Chemistry II (Second Edition)* 271–310 (Elsevier, 2013).

(23) Peña, O. Chevrel phases: Past, present and future. *Physica C* **2015**, *514*, 95–112.

(24) Delmas, C.; Fouassier, C.; Hagenmuller P. Structural Classification and Properties of the Layered Oxides. *Physica B + C* **1980**, *99 (1–4)*, 81–85.

(25) Petříček, V.; Dušek, M.; Palatinus, L. Crystallographic Computing System JANA2006: General Features. *Z. Für Krist. - Cryst. Mater.* **2014**, *229* (5), 345–352.

(26) Juhas, P.; Davis, T.; Farrow, C. L.; Billinge, S. J. L. PDFgetX3: A Rapid and Highly Automatable Program for Processing Powder Diffraction Data into Total Scattering Pair Distribution Functions *J. Appl. Cryst.* **2013**, *46*, 560–566.

(27) Farrow, C. L.; Juhas, P.; Liu, J. W.; Bryndin, D.; Bozin, E. S.; Bloch, J.; Proffen, T.; Billinge, S. J. L. PDFfit2 and PDFgui: Computer Programs for Studying Nanostructure in Crystals. *J. Phys.: Condens. Matter* **2007**, *19 (33)*, 335219.

(28) Perdew, J. P.; Burke, K.; Ernzerhof, M. Generalized Gradient Approximation Made Simple. *Phys. Rev. Lett.* **1996**, *77*, 3865–3868.

(29) Kresse, G.; Joubert, D. From Ultrasoft Pseudopotentials to the Projector Augmented-Wave Method. *Phys. Rev. B* **1999**, *59*, 1758–1775.

(30) Kresse, G.; Furthmüller, J. Efficient Iterative Schemes for Ab Initio Total-Energy Calculations using A Plane-Wave Basis Set. *Phys. Rev. B* **1996** *54*, 11169–11186.

(31) Bader, R. F. Atoms in molecules: a quantum theory. (Clarendon Pr, 1990).

(32) Tang, W.; Sanville, E. ; Henkelman, G. A grid-based Bader Analysis Algorithm without Lattice Bias. *J. Phys. Condens. Matter* **2009** *21*, 84204.

(33) Sanville, E.; Kenny, S. D.; Smith, R.; Henkelman, G. Improved Grid-Based Algorithm for Bader Charge Allocation. *J. Comput. Chem.* **2007**, *28*, 899–908.

(34) Henkelman, G.; Arnaldsson, A.; Jónsson, H. A Fast and Robust Algorithm for Bader Decomposition of Charge density. *Comput. Mater. Sci.* **2006**, *36*, 354–360.

(35) Becke, A. D.; Edgecombe, K. E. A Simple Measure of Electron Localization in Atomic and Molecular Systems. *J. Chem. Phys.* **1990**, *92 (9)*, 5397–5403.

(36) Momma, K.; Izumi, F. *VESTA 3* for Three-Dimensional Visualization of Crystal, Volumetric and Morphology Data. *J. Appl. Crystallogr.* **2011**, *44*, 1272–1276.

(37) Delmas, C.; Braconnier, J.-J.; Maazaz, A.; Hagenmuller, P. Soft Chemistry in A_xMO_2 Sheet Oxides. *Rev. Chim. Minérale* **1982**, *19*, 343–351.

(38) Peierls, R. *Quantum theory of solids*. (Oxford Univ. Press, 2001).

(39) Lamfers, H. J.; Meetsma, A.; Wiegers, G. A.; de Boer, J. L. The Crystal Structure of some Rhenium and Technetium Dichalcogenides. *J. Alloys Compd.* **1996**, *241*, 34–39.

(40) Alcock, N. W.; Kjekshus, A. The Crystal Structure of ReS_2. *Acta Chem. Scand.* **1965**, *19 (1)*, 79–94.

(41) Wildervanck, J. C.; Jellinek, F. The Dichalcogenides of Technetium and Rhenium. *J. Less -Common Met.* **1971**, *24 (1)*, 73–81.

(42) Murray, H. H.; Kelty, S. P.; Chianelli, R. R. Structure of Rhenium Disulfide. *Inorg. Chem.* **1994**, *33*, 4418–4420.

(43) Friemelt, K.; S. Akari, S.; Lux-Steiner, M.-C.; Schill, T.; Bucher, E.; Dransfeld, K. Scanning Tunneling Microscopy with Atomic Resolution on ReS_2 Single Crystals grown by Vapor Phase Transport. *Ann. Phys.* **1992**, *504*, 248–253.

(44) Guillevic, J. ; Le Marouille, J.-Y. ; Grandjean, D. Etude Structurale de Combinaisons Sulfurées et Séléniées du Molybdène. IV. Structures Cristallines de $CoMo_2S_4$ et de $FeMo_2S_4$. *Acta Crystallogr. B* **1974**, *30*, 111–117.

(45) Deblieck, R.; Van Landuyt, J.; Van Dyck, D.; Van Tendeloo, G.; Amelinckx, S. The Modulated Structure of $Mo_{2.065}S_3$. *J. Solid State Chem.* **1987**, *70 (1)*, 108–120.

(46) Dungey, K. E.; Curtis, M. D.; Penner-Hahn, J. E. Structural Characterization and Thermal Stability of MoS_2 Intercalation Compounds. *Chem. Mater.* **1998**, *10 (8)*, 2152–2161.

(47) Petkov, V.; Billinge, S. J. L.; Larson, P.; Mahanti, S. D.; Vogt, T.; Rangan, K. K.; Kanatzidis, M. G. Structure of Nanocrystalline Materials using Atomic Pair Distribution Function Analysis: Study of $LiMoS_2$. *Phys. Rev. B* **2002**, *65*, 092105.

(48) Kertesz, M.; Hoffmann, R. Octahedral vs Trigonal-Prismatic Coordination and Clustering in Transition-Metal Dichalcogenides. *J. Am. Chem. Soc.* **1984**, *106*, 3453–3460.

(49) Canadell, E., LeBeuze, A., El Khalifa, M. A., Chevrel, R.; Whangbo, M. H. Origin of Metal Clustering in Transition-Metal Chalcogenide Layers MX_2 (M= Nb, Ta, Mo, Re; X= S, Se). *J. Am. Chem. Soc.* **111,** 3778–3782 (1989).

(50) Fang, C. M.; Wiegers, G. A.; Haas, C.; de Groot, R. A. Electronic Structures of ReS_2, $ReSe_2$ and TcS_2 in the Real and the Hypothetical Undistorted Structures. *J. Phys. Condens. Matter* **1997**, *9 (21)*, 4411–4424.

(51) Roquefelte, X.; Boucher, F.; Gressier, P.; Ouvrard, G. Mo Cluster Formation in the Intercalation Compound $LiMoS_2$. *Phys. Rev. B* **2000**, *62 (4)*, 2397–2400.

(52) He, H.; Lu, P.; Wu, L.; Zhang, C.; Song, Y.; Guan, P.; Wang, S. Structural Properties and Phase Transition of Na Adsorption on Monolayer MoS_2. Nanoscale Res. Lett. 11, (2016).

(53) Aleandri, L. E.; McCarley, R. E. Hexagonal $LiMoO_2$: A Close-Packed Layered Structure with Infinite Mo-Mo-Bonded Sheets. *Inorg. Chem.* **1988**, *27 (6)*, 1041–1044.

(54) Ben-Kamel, K.; Amdouni, N.; Groult, H.; Mauger, A.; Zaghib, K.; Julien, C. M. Structural and electrochemical properties of $LiMoO_2$. *J. Power Sources* **2012**, *202*, 314–321.

(55) Hibble, S. J.; Fawcett, I. D. Local Order and Metal-Metal Bonding in Li_2MoO_3, $Li_4Mo_3O_8$, $LiMoO_2$, and H_2MoO_3, Determined from EXAFS Studies. *Inorg. Chem.* **1995**, *34 (2)*, 500–508.

(56) Hibble, S. J.; Fawcett, I. D.; Hannon, A. C. The True Structure and Metal-Metal-Bonded Framework of $LiMo^{III}O_2$ Determined from Total Neutron Scattering. *Inorg. Chem.* **1997**, *36 (9)*, 1749–1753.
(57) Shannon, R. D. Revised Effective Ionic Radii and Systematic Studies of Interatomic Distances in Halides and Chaleogenides. *Acta Cryst. A* **1976**, *32*, 751–767.
(58) Mikhailova, D.; Bramnik, N. N.; Bramnik, K. G.; Reichel, P.; Oswald, S.; Senyshyn, A.; Trots, D. M.; Ehrenberg, H. Layered Li_xMoO_2 Phases with Different Composition for Electrochemical Application: Structural Considerations. *Chem. Mater.* **2011**, *23*, 3429–3441.
(59) Assadi, M. H. N.; Shigeta, Y. The effect of octahedral distortions on the electronic properties and magnetic interactions in O3 $NaTMO_2$ compounds (TM = Ti–Ni & Zr–Pd). *RSC Adv.* **2018**, *8*, 13842–13849.

FOR TABLE OF CONTENT ONLY

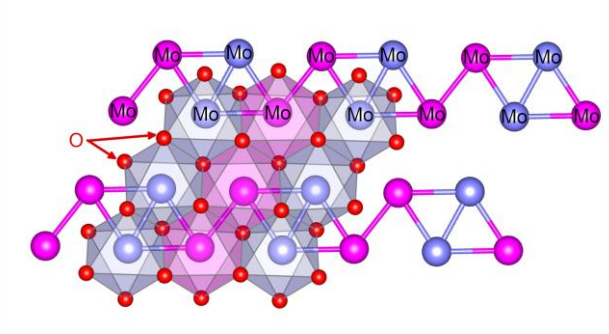

Chains of “diamond-like” clusters of molybdenum existing in $NaMoO_2$ in the $[MoO_2]$ layers formed by edge-sharing MoO_6 octahedra.